Computational Studies of the Mechanism for Proton and Hydride Transfer in Liver Alcohol Dehydrogenase

Pratul K. Agarwal, Simon P. Webb, and Sharon Hammes-Schiffer*

Contribution from the Department of Chemistry and Biochemistry, University of Notre Dame, Notre Dame, Indiana 46556-5670

Received December 21, 1999. Revised Manuscript Received March 2, 2000

Abstract: In this paper we present computational studies directed at elucidating the mechanism of the oxidation of benzyl alcohol by liver alcohol dehydrogenase (LADH). This enzyme reaction involves a hydride transfer from the alcohol substrate to the nicotinamide adenine dinucleotide coenzyme and a proton relay that deprotonates the alcohol substrate. Electronic structure calculations at various levels of theory were performed on a 148-atom model of the active site, and classical molecular dynamics simulations were performed on the entire solvated LADH dimer. These calculations support the hypothesis that alcohol deprotonation occurs prior to the hydride transfer step and that the alcohol deprotonation facilitates the hydride transfer by lowering the barrier for hydride transfer. In this postulated mechanism, the alcohol deprotonation leads to a zinc-bound alkoxide ion, and the subsequent hydride transfer leads to the benzaldehyde product. The calculations indicate that the zinc-bound alkoxide forms a strong hydrogen bond to Ser48 and that hydride transfer is accompanied by a weakening of this hydrogen bond. The results also suggest that the barrier to hydride transfer is lowered by the electrostatic interaction between the substrate alkoxide oxygen and the zinc counterion in the active site. The interaction of the alkoxide oxygen lone pair orbitals with the zinc competes with the formation of the double bond required for the aldehyde product, resulting in an earlier, more alcohol-like transition state and thus a lower activation energy barrier. In addition, the interaction between the alkoxide oxygen and the zinc restricts the dynamical motion of the substrate, decreasing the average donor−acceptor distance for hydride transfer and hence lowering the activation energy barrier.

Introduction

Liver alcohol dehydrogenase (LADH) catalyzes the reversible oxidation of alcohols to the corresponding aldehydes or ketones by the coenzyme nicotinamide adenine dinucleotide (NAD^+). The active enzyme has a molecular weight of 80 000 and is a dimer of two identical subunits. Each subunit contains one coenzyme-binding site, one active site, and two zinc ions, one of which is in the active site and is essential for catalysis. Numerous three-dimensional structures of horse liver alcohol dehydrogenase (HLADH) with the coenzyme and different substrates have been determined crystallographically. Figure 1 provides a schematic picture of the active site of HLADH based on the X-ray crystallographic structure of Ramaswamy, Eklund, and Plapp.[1] This crystal structure indicates that the substrate is coordinated to the catalytic zinc ion, which is also coordinated to Cys46, Cys174, and His67. The most widely accepted mechanism for alcohol oxidation by LADH is as follows:[2,3] (1) binding of the coenzyme NAD^+; (2) binding of the alcohol substrate by coordination to zinc; (3) deprotonation of the alcohol, leading to a zinc-bound alkoxide ion; (4) hydride transfer from the alkoxide ion to NAD^+, leading to NADH and a zinc-bound aldehyde or ketone; (5) release of the product aldehyde; (6) dissociation of NADH. In this paper we will focus on the third and fourth steps of this mechanism, namely, the proton and hydride transfer reactions.

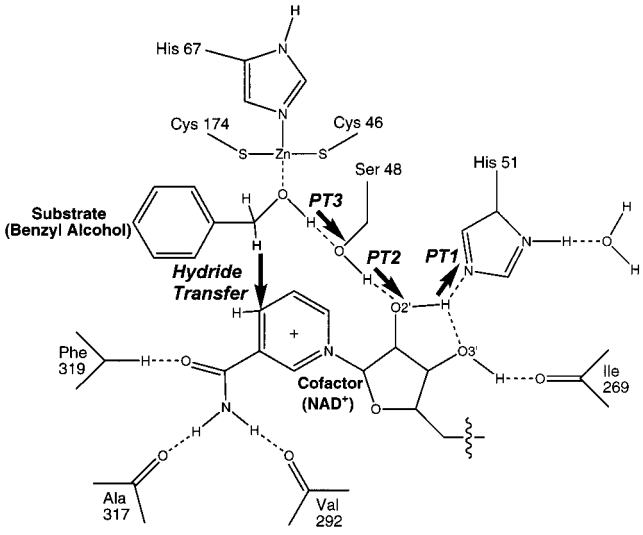

Figure 1. Schematic illustration of the active site of LADH with a benzyl alcohol substrate and an NAD^+ cofactor. The dark arrows indicate the hydride transfer reaction and the first three steps of the proton relay (denoted PT1, PT2, and PT3).]

Experimental studies have revealed a wealth of information about the proton and hydride transfer reactions involved in the LADH mechanism. Estimates of the relevant rate constants have been obtained from kinetic studies.[4] The hydride transfer is known to occur directly between the substrate and the NAD^+,

* Corresponding author. E-mail: hammes-schiffer.1@nd.edu.

(1) Ramaswamy, S.; Eklund, H.; Plapp, B. V. *Biochemistry* **1994**, *33*, 5230.

(2) Klinman, J. P. *Crit. Rev. Biochem.* **1981**, *10*, 39.

(3) Pettersson, G. *Crit. Rev. Biochem. Mol. Biol.* **1987**, *21*, 349.

(4) Shearer, G. L.; Kim, K.; Lee, K. M.; Wang, C. K.; Plapp, B. V. *Biochemistry* **1993**, *32*, 11186.

10.1021/ja994456w CCC: $19.00
Published on Web 04/26/2000

but the mechanism of proton transfer is not as well characterized. The crystal structures of Eklund and co-workers[5] and of Ramaswamy and co-workers[1] suggest a proton relay pathway in which the proton is transferred to His51 through a hydrogen-bonded system containing the hydroxyl groups of Ser48 and the nicotinamide ribose. (See Figure 1.) Reference 1 proposes several mechanisms by which the proton could be transferred from His51 to the aqueous solvent.

Experiments have also provided insight into the relationship between the proton relay and the hydride transfer. Kvassman and Pettersson[6,7] studied the pH dependence of the LADH reaction and found that their data are consistent with a mechanism in which the deprotonation of the alcohol occurs prior to the hydride transfer. They postulate that the pK_a of the alcohol substrate is lowered due to coordination to zinc, hydrogen bonding to Ser48, and electrostatic interaction with NAD^+. Most important, they suggest that the formation of the alkoxide lowers the barrier for hydride transfer. According to this hypothesis, the deprotonation of the alcohol substrate facilitates the hydride transfer reaction. Schmidt and co-workers[8] found that there is no solvent deuterium isotope effect on the hydride transfer step during aldehyde reduction, implying that the proton and hydride transfer steps are stepwise rather than concerted. In contrast, recently Ramaswamy, Park, and Plapp[9] found a significant inverse solvent deuterium isotope effect on the hydride transfer step during oxidation of benzyl alcohol, indicating that hydride transfer is accompanied by proton movement. In ref 9, these experimental data are interpreted as suggesting that the reactant state of LADH-catalyzed oxidation of benzyl alcohol involves a zinc-bound alkoxide ion with a low-barrier hydrogen bond to the hydroxyl group of Ser48.

A number of theoretical methods have been used to study alcohol oxidation in LADH.[10−18] Semiempirical and *ab initio* calculations on small model systems have centered on the roles of zinc, the Ser48 residue, and water. Onciul and Clark[10] have performed semiempirical AM1 calculations on small model systems of the active site including derivatives of Ser48, His51, and NAD^+ and a zinc ion coordinated to derivatives of Cys46, Cys174, His67, and ethanol. They studied a proton relay mechanism involving proton transfer from the ethanol to His51 through Ser48, without the inclusion of the nicotinamide ribose hydroxyl group shown in Figure 1. Their studies suggest that the alcohol proton is transferred directly to Ser48 rather than by way of a water molecule. The latter mechanism would involve a pentacoordinated zinc intermediate in which both the water and substrate are coordinated to zinc. They also studied hydride transfer from ethanolate to a model compound for NAD^+ and found that the hydride transfer step is rate limiting. Vanhommerig and co-workers[13] performed semiempirical AM1 and PM3 calculations on similar model systems with a different treatment of the cysteine ligands. Their studies also indicate that the pentacoordinated zinc intermediate would be energetically unfavorable. Tapia and co-workers performed *ab initio* calculations on somewhat smaller models to investigate the role of zinc, the geometry and electronic structure of the transition state for hydride transfer, and the effects of Ser48.[14,15] These theoretical studies suggest that the alcohol substrate replaces a zinc-bound water molecule upon binding, leading to a four-coordinate zinc for the catalytic reaction.

Molecular dynamics simulations of LADH are consistent with the conclusions from the semiempirical and *ab initio* calculations. Ryde performed molecular dynamics simulations on a portion of LADH (including up to 1224 atoms) with a four- and a five-coordinate catalytic zinc ion. These simulations indicate that a four-coordinate catalytic zinc ion is more stable than a five-coordinate one in LADH.[16] More recently Ryde reached similar conclusions based on mixed quantum mechanical/molecular mechanical simulations of LADH.[17]

Olson and co-workers[19] investigated the oxidation of an aldehyde to a carboxylic acid catalyzed by LADH. They performed semiempirical PM3 calculations on small model systems of the active site of LADH and molecular dynamics simulations on the LADH dimer. Their results suggest that the proton shuttle shown in Figure 1 represents a stepwise reaction which occurs subsequent to hydride transfer for aldehyde oxidation. Note that these conclusions are not directly relevant to the reaction studied in this paper (i.e., the oxidation of an alcohol to an aldehyde or ketone).

The theoretical studies presented in this paper are directed at further elucidating the mechanism of proton and hydride transfer in LADH-catalyzed alcohol oxidation. The specific reaction studied is the HLADH-catalyzed oxidation of benzyl alcohol to benzaldehyde. The proton and hydride transfer steps are illustrated in Figure 1. The hydride is transferred directly from the alcohol substrate to the NAD^+ coenzyme. We include only the first three steps of the proton relay mechanism suggested by the crystal structure in ref 1. This proton relay mechanism involves the following proton transfer steps: (1) the nicotinamide ribose to His51, (2) Ser48 to the nicotinamide ribose, and (3) the substrate alcohol to Ser48. Note that this is the same pathway studied in ref 19 for aldehyde oxidation but differs from the pathways previously studied for alcohol oxidation catalyzed by LADH.[10,13]

We utilize a variety of theoretical methods to investigate these charge-transfer steps. We performed semiempirical PM3, *ab initio*, and density functional theory (DFT) calculations on both a 43-atom model and a 148-atom model of the active site. The latter model is significantly larger than previously studied models. Localized molecular orbital (LMO) and partial charge analyses based on these electronic structure calculations provide useful insight into the mechanism. In addition, we performed molecular dynamics simulations on the entire solvated LADH dimer with both an alcohol and an alkoxide substrate. The results of these calculations support the hypothesis that the proton transfer occurs prior to the hydride transfer and that the alcohol deprotonation facilitates the subsequent hydride transfer. Moreover, these studies provide insight into the electronic and dynamical factors that lead to a lowering of the hydride transfer barrier after alcohol deprotonation.

(5) Euklund, H.; Plapp, B. V.; Samama, J.-P.; Branden, C. *J. Biol. Chem.* **1982**, *257*, 14359.
(6) Kvassman, J.; Pettersson, G. *Eur. J. Biochem.* **1980**, *103*, 557.
(7) Kvassman, J.; Pettersson, G. *Eur. J. Biochem.* **1980**, *103*, 565.
(8) Schmidt, J.; Chen, J.; DeTraglia, M.; Minkel, D.; McFarland, J. T. *J. Am. Chem. Soc.* **1979**, *101*, 3634.
(9) Ramaswamy, S.; Park, D.-H.; Plapp, B. V. *Biochemistry* **1999**, *38*, 13951.
(10) von Onciul, A. R.; Clark, T. *J. Comput. Chem.* **1993**, *14*, 392.
(11) de Kok, P. M. T.; Beijer, N. A.; Buck, H. M.; Sluyterman, L. A. A.; Meijer, E. M. *Eur. J. Biochem.* **1988**, *175*, 581.
(12) Beijer, N. A.; Buck, H. M.; Sluyterman, L. A. A.; Meijer, E. M. *Biochim. Biophys. Acta* **1990**, *1039*, 227.
(13) Vanhommerig, S. A. M.; Meier, R. J.; Sluyterman, L. A.; Meijer, E. M. *J. Mol. Struct.: THEOCHEM* **1996**, *364*, 33.
(14) Tapia, O.; Cardenas, R.; Andrés, J.; Krechl, J.; Campillo, M.; Colonna-Cesari, F. *Int. J. Quantum Chem.* **1991**, *39*, 767.
(15) Cárdenas, R.; Andrés, J.; Krechl, J.; Campillo, M.; Tapia, O. *Int. J. Quantum Chem.* **1996**, *57*, 245.
(16) Ryde, U. *Proteins: Struct., Funct., Genet.* **1995**, *21*, 40.
(17) Ryde, U. *J. Comput.-Aided Mol. Des.* **1996**, *10*, 153.
(18) Ryde, U. *Eur. Biophys. J.* **1996**, *24*, 213.
(19) Olson, L. P.; Luo, J.; Almarsson, Ö.; Bruice, T. C. *Biochemistry* **1996**, *35*, 9782.

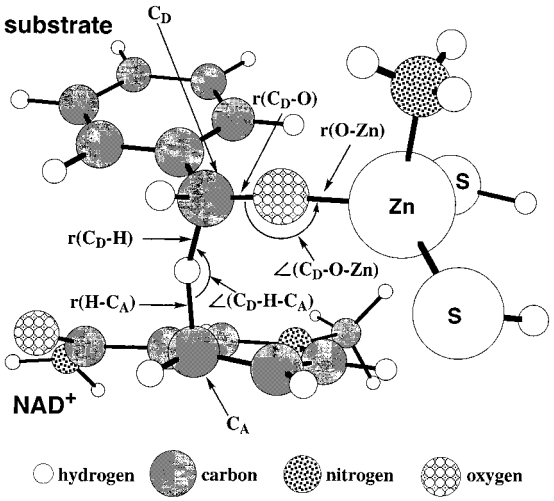

Figure 2. Transition state for the smaller 43-atom model of the LADH active site. Bond lengths and angles are labeled for use in Table 1. The donor and acceptor carbon atoms for the hydride transfer are denoted C_D and C_A, respectively.

Methods

Electronic Structure Calculations. Electronic structure calculations were carried out using the semiempirical PM3 method, the restricted Hartree−Fock (RHF) method, and DFT. Basis sets utilized are the standard double-ζ quality basis sets 3-21G[20−22] and 6-31G**.[23−25] The 6-31G* basis set for Zn was recently developed and includes f polarization functions.[26] In addition, a triple-ζ basis set with d and p polarization functions (no f polarization on Zn) denoted TZV(d,p),[27−30] was employed.

Calculations were performed on two different models of the active site of LADH. The smaller 43-atom model includes analogues of three protein residues (Cys46, His67, and Cys174), the catalytic zinc ion, the substrate benzyl alcohol, and a coenzyme NAD^+ analogue. This model has no overall charge and is shown in Figure 2. The larger 148-atom model includes analogues of nine protein residues (Cys46, Ser48, His51, His67, Cys174, Ile269, Val292, Ala317, and Phe319), the catalytic zinc ion, the substrate benzyl alcohol, a coenzyme NAD^+ analogue, and a water molecule. The water molecule was included to prevent the His51 ring from flipping. The hydrophobic side chains of protein residues which do not participate in the reaction were truncated to reduce the number of atoms in the model. The analogues used for the amino acids and coenzyme in the larger model are depicted in Figure 3. The overall charge for the larger model is +1.

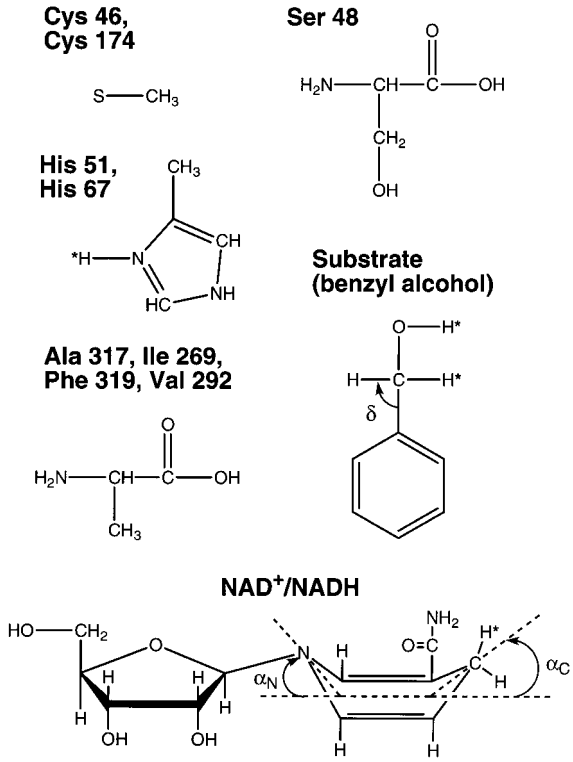

Figure 3. Analogues for the amino acids, the NAD^+ coenzyme, and the alcohol substrate used in the larger 148-atom model of the LADH active site depicted in Figure 1. The asterisks denote the hydrogen atoms that may be transferred. The angles δ, α_C, and α_N are labeled for use in the text and tables.

Calculations on the 43-atom model were carried out to give an indication of the reliability of the basis sets and methods used for the larger 148-atom model. Transition-state searches at the PM3, RHF/3-21G, RHF/6-31G**, RHF/TZV(d,p), and DFT/B3LYP/6-31G** levels of theory were performed to investigate basis set and electron correlation effects on geometry. The PM3 and 3-21G transition-state structures were confirmed as such by calculation of the energy second derivative (Hessian) followed by diagonalization to yield one negative eigenvalue. For PM3 the Hessian was determined numerically (double displacement); for RHF/3-21G it was determined analytically. In addition, optimizations of constituent anion and cation minima and single-point energy calculations were performed at various levels of theory to test the sensitivity of relative energies to the basis set, electron correlation, and geometry.

Due to the large size of the 148-atom model, the PM3 semiempirical method was utilized to generate initial potential energy surfaces for the hydride and three proton transfer reactions. This was done by first determining transition state structures and then generating minimum energy paths (MEPs) to their associated reactant and product using the intrinsic reaction coordinate method of Gonzales and Schlegel.[35] The starting point for these calculations was the determination of the transition state for the hydride transfer step. Initial coordinates for this transition-state geometry search were obtained from the crystal structure in ref 1. Initial structures for subsequent proton transfer transition-state geometry searches were obtained from relevent minima generated as described above. All stationary points found at the PM3 level were

(20) Binkley, J. S.; Pople, J. A.; Hehere, W. J. *J. Am. Chem. Soc.* **1980**, *102*, 939.
(21) Gordon, M. S.; Binkley, J. S.; Pople, J. A.; Pietro, W. J.; Hehre, W. J. *J. Am. Chem. Soc.* **1983**, *104*, 2797.
(22) Dobbs, K. D.; Hehre, W. J. *J. Comput. Chem.* **1987**, *8*, 861.
(23) Ditchfield, R.; Hehre, W. J.; Pople, J. A. *J. Chem. Phys.* **1971**, *54*, 724.
(24) Hehre, W. J.; Ditchfield, R.; Pople, J. A. *J. Chem. Phys.* **1972**, *56*, 2257.
(25) Francl, M. M.; Petro, W. J.; Hehre, W. J.; Binkley, J. S.; Gordon, M. S.; DeFrees, D. J.; Pople, J. A. *J. Chem. Phys.* **1982**, *77*, 3654.
(26) Rassolov, V.; Pople, J. A.; Ratner, M.; Windus, T. L. *J. Chem. Phys.* **1998**, *109*, 1223.
(27) Dunning, T. H. *J. Chem. Phys.* **1971**, *55*, 716.
(28) McLean, A. D.; Chandler, G. S. *J. Chem. Phys.* **1980**, *72*, 5639.
(29) Wachters, A. J. H. *J. Chem. Phys.* **1970**, *52*, 1033.
(30) Rappe, A. K.; Smedley, T. A.; Goddard, W. A., III. *J. Phys. Chem.* **1981**, *85*, 2607.
(31) Becke, A. D. *J. Chem. Phys.* **1993**, *98*, 1372.
(32) Stephens, P. J.; Devlin, F. J.; Chabalowski, C. F.; Frisch, M. J. *J. Phys. Chem.* **1994**, *98*, 11623.
(33) Becke, A. D. *Phys. Rev. A* **1988**, *38*, 3098.
(34) Lee, C.; Yange, W.; Parr, R. G. *Phys. Rev. B* **1988**, *37*, 785.
(35) Gonzales, C.; Schlegel, H. B. *J. Chem. Phys.* **1989**, *90*, 2154.

characterized by numerical (double displacement) calculation of the Hessian, diagonalization, and inspection of the eigenvalues (where one negative eigenvalue indicates a transition state and no negative eigenvalues indicates a minimum). The PM3 parametrization was chosen over the AM1 parametrization since the PM3 model has been found to be much better at reproducing hydrogen bond geometries.[36] Moreover, a previous comparison of AM1 and PM3 for small model systems of the LADH active site indicates that although the energies differ, the optimized geometries are almost identical with AM1 and PM3.[13]

RHF/3-21G geometry searches for the 148-atom model were performed for the hydride transfer step only. The relevant PM3 stationary point geometries were used as initial structures for computational efficiency. In addition, single-point RHF/6-31G** and DFT/B3LYP/6-31G** energies at the RHF/3-21G-optimized structures (denoted RHF/6-31G**//3-21G and DFT/B3LYP/6-31G**//3-21G, respectively) were carried out.

Interpretation of the wave functions resulting from these electronic structure calculations was aided by the determination of partial charges and the localization of molecular orbitals. The CHELPG method was used to calculate the partial charges.[37] The Boys method,[38] which involves maximization of the sum of the distances between orbital centroids, was used to localize the canonical molecular orbitals generated at the RHF/3-21G level. This enabled an analysis of the bonding in terms of the more physically intuitive LMOs.

Several different electronic structure packages were utilized for these calculations. All PM3 calculations, 43-atom model RHF calculations, and 148-atom model RHF/3-21G transition-state searches were carried out using the electronic structure package GAMESS.[39] The 43-atom model DFT calculations plus the 148-atom model RHF/3-21G minimum geometry searches were carried out using Gaussian98.[40] The RHF/6-31G**//PM3, DFT/B3LYP/6-31G**//PM3, RHF/6-31G**//RHF/3-21G, and DFT/B3LYP/6-31G**//RHF/3-21G single-point energy calculations for the 148-atom model were carried out using Q-Chem.[41] All energy and energy gradient convergence criteria used were defaults in the particular software package used except for the RHF/3-21G transition-state geometry searches, where the energy gradient convergence criterion was relaxed an order of magnitude to a maximum of 0.001 hartree/bohr and an RMS of one-third of this. (In addition, one of the transition states was also obtained with the energy gradient convergence criterion set to a maximum of 0.0005 hartree/bohr and an RMS of one-third of this.)

Molecular Dynamics Simulations. Molecular dynamics simulations were performed on the solvated LADH dimer with the GROMOS biomolecular simulation program.[42] The model for each monomer included all 374 amino acid residues, the coenzyme NAD^+, the substrate benzyl alcohol (or intermediate benzyl alkoxide), and the water molecules found in the crystal structure. The initial coordinates were obtained from the crystal structure presented in ref 1. The system was placed in a rectangular water box with periodic boundary conditions, and the dimensions of the box were chosen such that the minimum distance between the solute and the side of the box was 8 Å. A cutoff radius of 14 Å was used for the nonbonded interactions. All atoms in the system were allowed to move during the minimizations and the molecular dynamics simulations. The bonds involving hydrogens were constrained using the SHAKE algorithm.[43]

The standard GROMOS parameters were used for the protein residues, and the SPC/E model was used to describe the water molecules. The partial charges for the substrate (benzyl alcohol and benzyl alkoxide) were obtained from CHELPG[37] analyses based on *ab initio* calculations at the RHF/6-31G** level. Polar hydrogens were added to the protein residues, coenzyme, and substrate. The two hydrogen atoms on the α-carbon of the alcohol were also added. The united atom approach was used for the remaining atoms. The protonation states of the histidines and the cysteines were chosen to be the same as in ref 16. A bonded approach was used to describe the interaction of the amino acid ligand atoms and the zinc ions to maintain appropriate geometries around the zinc ions. The substrate ligands were allowed to interact solely by nonbonded potentials. The equilibrium bond lengths and angles, as well as the force constants, for the zinc−ligand bonds were obtained from the parametrization of the zinc ion in HLADH developed by Ryde.[16] For simplicity the noncatalytic zinc bonding terms included only distance restraints.

The system was equilibrated prior to the collection of molecular dynamics data. Each equilibration step consisted of a steepest descent energy minimization (with an energy threshold of 0.024 kcal/mol) followed by a 5 ps molecular dynamics simulation. Harmonic positional restraints were applied during these equilibration steps. The initial force constant was 100 kcal/mol and was scaled by 0.5 after each equilibration step. After four equilibration steps of this type (with force constants of 100, 50, 25, and 12.5 kcal/mol), the final equilibration step was performed without any positional restraints. The duration of this final step was chosen to ensure equilibration. The time step for all molecular dynamics simulations was 1 fs, and the temperature was 300 K.

Results and Discussion

The aim of the computational studies presented in this paper is to elucidate the mechanism of proton and hydride transfer in the LADH-catalyzed oxidation of benzyl alcohol. First we describe electronic structure calculations on the 43-atom model system to provide an indication of the reliability of the basis sets and methods for these types of systems. Then we present electronic structure calculations on the larger 148-atom model of the enzyme active site. In addition to discussing the entire

(36) Schröder, S.; Daggett, V.; Kollman, P. *J. Am. Chem. Soc.* **1991**, *113*, 8922.

(37) Breneman, C. M.; Wiberg, K. B. *J. Comput. Chem.* **1990**, *11*, 361.

(38) Boys, F. S. *The Quantum Theory of Atoms, Molecules and Solids*; Academic Press: New York, 1966.

(39) Schmidt, M. W.; Baldridge, K. K.; Boatz, J. A.; Elbert, S. T.; Gordon, M. S.; Jensen, J. H.; Koseki, S.; Matsunaga, N.; Nguyen, K. A.; Su, S.; Windus, T. L.; Dupuis, M.; Montgomery, J. A. *J. Comput. Chem.* **1993**, *14*, 1347.

(40) Gaussian 98, Revision A.6: Frisch, M. J.; Trucks, G. W.; Schlegel, H. B.; Scuseria, G. E.; Robb, M. A.; Cheeseman, J. R.; Zakrzewski, V. G.; Montgomery, J. A., Jr.; Stratmann, R. E.; Burant, J. C.; Dapprich, S.; Millam, J. M.; Daniels, A. D.; Kudin, K. N.; Strain, M. C.; Farkas, O.; Tomasi, J.; Barone, V.; Cossi, M.; Cammi, R.; Mennucci, B.; Pomelli, C.; Adamo, C.; Clifford, S.; Ochterski, J.; Petersson, G. A.; Ayala, P. Y.; Cui, Q.; Morokuma, K.; Malick, D. K.; Rabuck, A. D.; Raghavachari, K.; Foresman, J. B.; Cioslowski, J.; Ortiz, J. V.; Stefanov, B. B.; Liu, G.; Liashenko, A.; Piskorz, P.; Komaromi, I.; Gomperts, R.; Martin, R. L.; Fox, D. J.; Keith, T.; Al-Laham, M. A.; Peng, C. Y.; Nanayakkara, A.; Gonzalez, C.; Challacombe, M.; Gill, P. M. W.; Johnson, B.; Chen, W.; Wong, M. W.; Andres, J. L.; Gonzalez, C.; Head-Gordon, M.; Replogle, E. S.; Pople, J. A., Gaussian, Inc., Pittsburgh, PA, 1998.

(41) Johnson, B. G.; Gill, P. M. W.; Head-Gordon, M.; White, C. A.; Baker, J.; Maurice, D. R.; Adams, T. R.; Kong, J.; Challacombe, M.; Schwegler, E.; Oumi, M.; Ochsenfeld, C.; Ishikawa, N.; Florián, J.; Adamson, R. D.; Dombroski, J. P.; Graham, R. L.; Warshel, A., Q-Chem, Inc., Export, PA, 1997.

(42) Scott, W. R. P.; Hünenberger, P. H.; Tironi, I. G.; Mark, A.; Billeter, S. R.; Fennen, J.; Torda, A. E.; Huber, T.; Krüger, P.; van Gunsteren, W. F. J. Phys. Chem. A **1999**, *103*, 3596.

(43) Ryckaert, J.-P.; Ciccotti, G.; Berendsen, H. J. C. *J. Comput. Phys.* **1977**, *23*, 327.

Table 1. Relevant Geometrical Values for the Transition State of the 48-Atom Model Obtained at Various Levels of Theory[a]

	$r(C_D-C_A)$ (Å)	$r(C_D-H)$ (Å)	$r(H-C_A)$ (Å)	$r(C_D-O)$ (Å)	$r(O-Zn)$ (Å)	$\angle(C_D-H-C_A)$ (deg)	$\angle(C_D-O-Zn)$ (deg)
PM3	2.86	1.32	1.55	1.31	2.05	173.8	131.7
RHF/3-21G	2.60	1.29	1.34	1.31	1.85	163.8	167.3
RHF/6-31G**	2.67	1.29	1.42	1.28	1.97	161.5	165.3
RHF/TZV(d,p)	2.68	1.29	1.43	1.28	2.00	162.5	165.0
DFT/B3LYP/6-31G**	2.70	1.26	1.47	1.31	1.97	162.9	152.8

[a] The parameters are defined in Figure 2.

Table 2. Energy of the Transition State of the 48-Atom Model Relative to the Separated NAD^+ Analogue $[C_7H_9ON_2]^+$ and Zinc-Bound Alkoxide $[C_7H_{12}ONZnS_2]^-$ Ions for Various Levels of Theory

	ΔE (kcal/mol)		ΔE (kcal/mol)
PM3	54.0	RHF/6-31G**//RHF/3-21G	48.3
RHF/3-21G	60.2	DFT/B3LYP/6-31G**//PM3	57.2
RHF/6-31G**	50.6	DFT/B3LYP/6-31G**//RHF/3-21G	71.0
DFT/B3LYP/6-31G**	72.3	DFT/B3LYP/6-31G**//RHF/6-31G**	71.1
RHF/6-31G**//PM3	24.7		

minimum energy path for the three proton transfer reactions and the hydride transfer reaction generated at the PM3 level, we describe higher level *ab initio* studies of the hydride transfer step. We present a detailed analysis of the geometries, energetics, and localized molecular orbitals for the hydride transfer step. Furthermore, after the discussion of these electronic structure calculations, we describe classical molecular dynamics simulations of the solvated LADH dimer. All of these computational studies provide insight into the mechanism of proton and hydride transfer in LADH.

We performed electronic structure calculations on the 43-atom model system to determine the reliability of a range of basis sets and methods for the description of intramolecular chemical interactions similar to many of those seen in the larger 148-atom model. Table 1 presents relevant geometrical values for hydride transfer transition states obtained for the 43-atom model using various levels of theory. As expected, PM3 provides the least reliable description, exhibiting considerable differences in geometry compared to the higher levels of theory. With respect to basis set effects, comparison of RHF/3-21G to RHF/6-31G** illustrates that the lower quality basis set leads to some geometrical differences: the C_D-C_A distance is shorter by 0.07 Å, the $H-C_A$ distance is shorter by 0.08 Å (while the C_D-H distance is unchanged), and the $Zn-O$ distance is shorter by 0.12 Å. Comparison of calculated parameters at the RHF/6-31G** and RHF/TZV(d,p) levels suggests that the 6-31G** basis set provides a good description of this system. With respect to electron correlation effects, comparison of RHF/6-31G** to DFT/B3LYP/6-31G** indicates that there is a small effect on the transition-state geometry, most notably for the C_D-H-C_A bond lengths, where the C_D-H and $H-C_A$ distances are shortened and lengthened by 0.03 and 0.05 Å, respectively, and the C_D-O-Zn angle, which is reduced by 12.5°.

In addition to establishing the basis set and correlation effects on the geometry of the 43-atom model, we also determined the sensitivity of the energies to the geometrical differences. For this purpose we calculated the energies of the transition states relative to the separated NAD^+ analogue $[C_7H_9ON_2]^+$ and zinc-bound alkoxide $[C_7H_{12}ONZnS_2]^-$ ions for the various levels of theory. The relative energies presented in Table 2 illustrate that geometries determined at the RHF/3-21G level provide an adequate basis for higher level single-point energy calculations for the 43-atom model. The calculated relative energies for RHF/6-31G**//RHF/3-21G and RHF/6-31G** differ by only 2.3 kcal/mol, and those for DFT/B3LYP/6-31G**//RHF/3-21G and DFT/B3LYP/6-31G** differ by only 1.3 kcal/mol. Thus, the geometrical differences between RHF/3-21G and higher levels of theory do not appear to have a large effect on relative energetics. In contrast, PM3 geometries do not provide an adequate basis for higher level single-point energy calculations. To summarize, we conclude that, while it is preferable to use geometries determined at the RHF/6-31G** level for higher level single-point energy calculations, the RHF/3-21G level provides reasonable geometries for such calculations in the case of the 43-atom model. Furthermore, given the chemical nature of the 43-atom model, we expect similar behavior in the 148-atom model.

The electronic structure calculations presented in the remainder of this paper are on the 148-atom model of the LADH active site. We used this 148-atom model to investigate two possible mechanisms for alcohol oxidation: in mechanism A the proton relay occurs prior to the hydride transfer, and in mechanism B the hydride transfer occurs prior to the proton relay. Although these two mechanisms assume the proton and hydride transfer reactions are sequential, we also analyzed the motion of the protons during the hydride transfer step to investigate the possibility of a concerted reaction. In addition, we emphasize that numerous transition states and minima with small geometrical differences at the periphery of the system exist for this relatively large model. Since these small geometrical differences are not expected to alter the overall qualitative mechanism, the structures presented in this paper can be viewed as representative of this large group of structures.

Despite the evident limitations of the PM3 method (see Tables 1 and 2), we used it to generate MEPs for mechanisms A and B. The relative inexpensiveness of the PM3 method allowed us to calculate the entire minimum energy path, including the three proton transfer reactions and the hydride transfer reaction, thereby providing a useful starting point for our study. The MEPs obtained with the PM3 semiempirical method for mechanisms A and B are shown in Figure 4. (Note that both MEPs are relative to the same zero of energy.) For both mechanisms, the MEPs for the individual reactions joined together in a way that resulted in the overall smooth MEP shown in Figure 4. In both cases the proton relay studied was stepwise with the three steps in the order indicated in Figure 1. These two mechanisms do not represent all possible ways in which a hydride and three protons can be transferred. For example, two or more of the steps could be concerted, and different orderings of the various steps could occur. Our search for other mechanisms involving concerted steps or a different ordering of the proton transfer steps, however, resulted in very high energy intermediate structures. The intermediate with only PT3 trans-

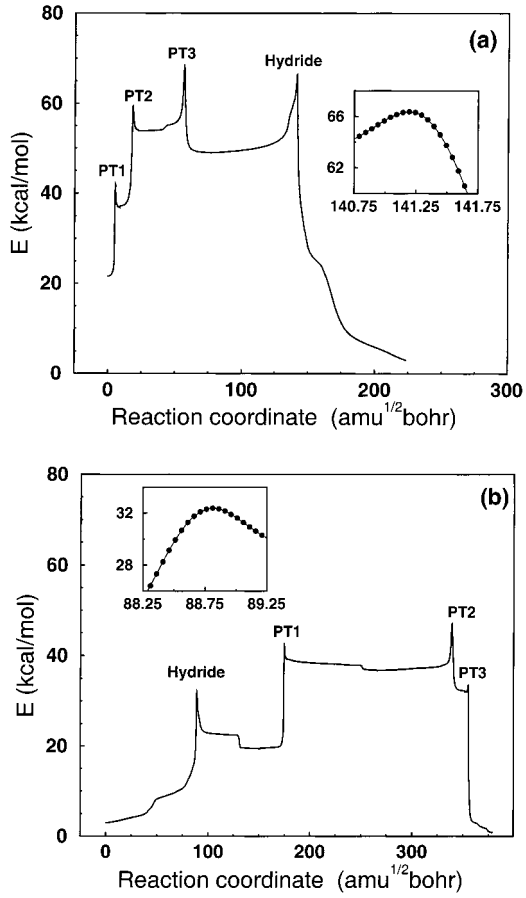

Figure 4. Minimum energy paths calculated with the semiempirical PM3 method for the 148-atom model for (a) mechanism A and (b) mechanism B. The transition states for the four reaction steps are labeled as in Figure 1. The insets depict magnifications of the hydride transfer step.

ferred is 24.6 kcal/mol higher than the intermediate with only PT1 transferred, and the intermediate with only PT2 transferred could not be located. The preference for the initial proton transfer step corresponding to PT1 rather than PT3 may be due to the high energy of a protonated alcohol ($SerOH_2^+$) relative to a protonated imidazole (His51). In addition, we observed that for each proton or hydride transfer step the other three nonreactive hydrogen atoms did not move significantly, suggesting a sequential mechanism at the PM3 level. (The average change in bond length for the nonreactive hydrogen atoms was found to be 0.01 Å.) A more detailed analysis of the energetics of these MEPs is problematic since, as shown in Tables 1 and 2, the PM3 energies are unreliable and the PM3 structures do not appear to be adequate for higher level single-point energy calculations.

To obtain more reliable structures, we performed calculations at the RHF/3-21G level. (As described above, calculations on the smaller 43-atom model indicate that the RHF/3-21G geometries are reasonable.) Due to the substantial computational cost, we determined only the reactant, transition state, and product structures for the hydride transfer step. Table 3 provides the important geometrical values for the reactant, transition state, and product structures for the hydride transfer step for both mechanisms at the RHF/3-21G level. The donor (substrate) and acceptor (NAD^+) carbon atoms for the hydride transfer are denoted C_D and C_A, respectively. As expected, the C_D-C_A distance in the transition state for hydride transfer is shorter than in the crystal structure (where this distance is 3.35 Å[1]). In addition, the C_D-H-C_A angles in the transition states are nearly

Table 3. Relevant Geometrical Values for the Reactant, Transition State, and Product Structures Obtained at the RHF/3-21G Level for Mechanism A and Mechanism B with the 148-Atom Model[a]

	mechanism A			mechanism B		crystal
	reactant	TS	product	reactant	TS	structure
C_D-C_A distance (Å)	3.74	2.59	4.18	4.59	2.58	3.35
C_D-H distance (Å)	1.09	1.30	3.49	1.09	1.35	
$H-C_A$ distance (Å)	3.62	1.30	1.08	5.13	1.24	
C_D-H-C_A angle (deg)	87.9	167.9	123.1	55.1	165.9	
Zn−O distance (Å)	1.88	1.93	1.92	3.37	5.11	2.05
PT1 distance (Å)	2.66	2.69	2.68	2.61	2.63	3.10
PT2 distance (Å)	2.44	2.55	2.63	2.60	2.54	2.76
PT3 distance (Å)	2.44	2.68	4.00	2.61	2.48	2.63
δ angle (deg)	108.4	112.6	116.2	108.9	115.6	
α_C angle (deg)	1.0	13.0	14.2	2.2	14.7	0.7
α_N angle (deg)	0.4	7.6	10.7	1.0	8.8	−1.3

[a] C_D and C_A represent the donor (substrate) and acceptor (NAD^+) carbon atoms, respectively, H represents the transferring hydride, and O represents the substrate oxygen ligated to the zinc in Figure 1. The PT1, PT2, and PT3 distances refer to the distance between the proton donor and acceptor for each proton transfer reaction, as labeled in Figure 1. The angles δ, α_C, and α_N are defined in Figure 3. The values from the crystal structure presented in ref 1 are given for comparison.

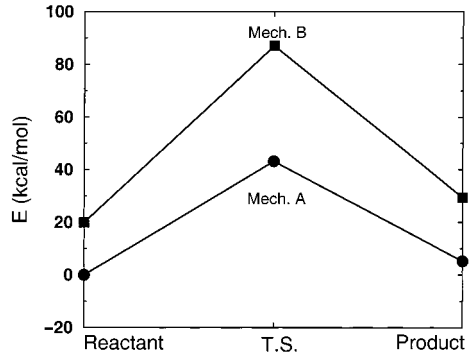

Figure 5. Relative energies for the reactant, transition state, and product for the hydride transfer reaction optimized at the RHF/3-21G level. The circles and squares represent the points for mechanism A and mechanism B, respectively.

linear for both mechanisms. The Zn−O distance is significantly larger for mechanism B than for mechanism A, as expected since for mechanism A the oxygen atom is deprotonated (i.e., the hydrogen on the oxygen for mechanism B decreases the electrostatic attraction between the oxygen and the zinc). Note that the Zn−O distance would not be allowed to become so large in the presence of the remainder of the enzyme (i.e., the large Zn−O distance for mechanism B is due to the limited size of the model system). Finally, we observed that the NADH ring puckering angles α_C and α_N in the product structure are slightly larger than those calculated for substituted 1,4-dihydropyridines by Wu and Houk.[44] This difference may be due to the inclusion of a portion of the enzyme active site environment in our 148-atom model.

The relative energies at the RHF/3-21G level for the hydride transfer steps of mechanisms A and B are shown in Figure 5. The RHF/6-31G**//RHF/3-21G and DFT/B3LYP/6-31G**//RHF/3-21G relative energies for reactants, transition states, and products are shown in Figure 6. The numerical values of the relative energies for the various levels of theory are given in Table 4. Note that we were unable to find a minimum representing the intermediate product for mechanism B (i.e., a structure in which the hydride is transferred but the protons involved in the proton relay are not transferred). Instead, we

(44) Wu, Y.-D.; Houk, K. N. *J. Am. Chem. Soc.* **1991**, *113*, 2353.

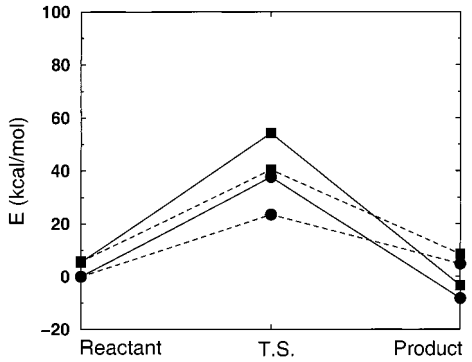

Figure 6. Single-point energies at the RHF/6-31G**//RHF/3-21G (solid line) and DFT/B3LYP/6-31G**//RHF/3-21G (dashed line) levels for the reactant, transition state, and product geometries. The circles and squares represent the points for mechanism A and mechanism B, respectively.

found that the proton relay occurred spontaneously after the transition state (i.e., there are no barriers to the proton relay, so the system progresses straight to a product similar to that in mechanism A, where all protons in the proton relay are transferred). The differences in the energies of the products for mechanism A and mechanism B are due to geometrical differences in other parts of the model. (Such relatively large systems contain numerous transition states and minima that differ mainly in the periphery of the model.) Note also that the calculated energies given in Table 4 do not include zero-point energy or entropy effects. Unfortunately, these effects cannot be included since an exact Hessian is unavailable at the RHF/3-21G level due to computational expense.

At all three levels of theory, mechanism A follows the lower energy path, and the activation energy barrier for hydride transfer is lower for mechanism A. Thus, all of these results suggest that mechanism A is more favorable than mechanism B. (Note that computer simulations have supported a similar mechanism for another enzyme, malate dehydrogenase.[45]) As illustrated by the calculations on the 43-atom model, although the structures obtained at the RHF/3-21G level are reasonable, the energetics are unreliable without inclusion of electron correlation. One indication of this unreliability is the prediction of an exothermic hydride transfer at the RHF/6-31G**//RHF/3-21G level, which is inconsistent with the experimental evidence that the alcohol reactant is favored at equilibrium.[46] The DFT/B3LYP/6-31G**//RHF/3-21G level of theory, which includes electron correlation, predicts an endothermic reaction and thus is qualitatively consistent with experiment. Moreover, neglecting the effects of zero-point energy and entropy, the barrier height and endothermicity obtained at the DFT/B3LYP/6-31G**//RHF/3-21G level for mechanism A (21.9 and 4.9 kcal/mol, respectively) agree qualitatively with the experimental free energies of activation and reaction (15 and 1 kcal/mol, respectively).

We have analyzed the motion of the protons involved in the proton relay during the hydride transfer step for mechanism A. The average change in bond length for the three protons during the hydride transfer reaction was found to be 0.03 Å. This observation suggests that the deprotonation and hydride transfer steps are sequential rather than concerted. As shown in Table 3, however, the distance between the substrate oxygen and the Ser48 oxygen (corresponding to PT3) is only 2.44 Å in the reactant state for mechanism A. Due to this very strong hydrogen bond, the order of the hydride transfer and the PT3 reaction is not well-defined. Moreover, we found that the distance between the proton and the Ser48 oxygen is 1.06, 0.99, and 0.98 Å for the reactant, transition state, and product structures for mechanism A. These results are consistent with the suggestion in ref 9 (based on the experimentally measured inverse solvent deuterium isotope effect) that the reactant is a zinc-bound alkoxide with a strong hydrogen bond to Ser48 and that the hydride transfer is accompanied by some proton motion (in this case, only ~0.08 Å). Note that, in related work, Turner, Moliner, and Williams[47] found that the transition state for the reduction of pyruvate by lactate dehydrogenase suggests proton motion during the hydride transfer. We emphasize that a more rigorous investigation of the relation between the proton and hydride transfer reactions requires a larger model, a higher level of electronic structure theory, and the quantum mechanical treatment of the transferring hydrogen nuclei. This is a direction for future research.

To elucidate the electronic differences between mechanism A and mechanism B, we analyzed the LMOs obtained with the Boys method.[38] Figures 7 and 8 illustrate the LMOs for mechanism A and mechanism B, respectively. In each figure, the left and right columns depict LMOs for the reactant and transition state structures, respectively. Although not shown, this analysis was also performed for the product structures.

Figure 7 presents the relevant LMOs for mechanism A. Parts a−h of Figure 7 depict the four LMOs involving the oxygen atom ligated to the zinc. Parts a and b of Figure 7 depict the LMOs representing a lone pair on this oxygen atom. These orbitals are virtually identical for the reactant and transition state structures. In both cases the lone pair is directly oriented toward the zinc. Parts c and d of Figure 7 depict the LMOs representing another lone pair on the oxygen atom. These orbitals are significantly different for the two structures. For the reactant structure this orbital is partially oriented toward the zinc, while for the transition state structure this orbital represents the early stages of a C_D-O π bond. Parts e and f of Figure 7 depict the LMOs representing a C_D-O σ bond and are very similar for the reactant and transition state structures. Parts g and h of Figure 7 depict the LMOs representing the hydrogen bond to Ser48. These LMOs are similar for the reactant and transition state structures, although small differences are observed due to the weakening of the hydrogen bond during the reaction. (This weakening of the hydrogen bond is consistent with the hypothesis that proton motion accompanies the hydride transfer.[9]) Parts i and j of Figure 7 depict the LMOs directly involved in the hydride transfer reaction. In the reactant this orbital represents a standard C_D-H bond, while in the transition state this orbital represents a two-electron three-center C_D-H-C_A bond. To summarize, this LMO analysis indicates that in the transition state one of the lone pairs on the oxygen atom forms the early stages of a C_D-O π bond. Although not shown, in the product the C_D-O double bond is completely formed, and the C_D-H-C_A bond in the transition state becomes a C_A-H bond.

In contrast to mechanism A, in mechanism B the zinc is far from the oxygen atom and thus is not involved in the hydride transfer step. As above, parts a−h of Figure 8 depict the four LMOs involving the oxygen atom. Parts a and b of Figure 8 depict the LMOs representing a lone pair on this oxygen atom. These orbitals are virtually identical for the reactant and transition state structures. Moreover, these orbitals differ from those for mechanism A in that they do not interact with the

(45) Cunningham, M. A.; Ho, L. L.; Nguyen, D. T.; Gillilan, R. E.; Bash, P. A. *Biochemistry* **1997**, *36*, 4800.

(46) Sekhar, V. C.; Plapp, B. V. *Biochemistry* **1990**, *29*, 4289.

(47) Turner, A. J.; Moliner, V.; Williams, I. H. *PCCP* **1999**, *1*, 1323.

Table 4. Relative Energies for the Hydride Transfer Reaction Calculated at the RHF/3-21G, RHF/6-31G**, and DFT/B3LYP/6-31G** Levels for Geometries Optimized at the RHF/3-21G level for Mechanism A and Mechanism B with the 148-Atom Model[a]

	RHF/3-21G		RHF/6-31G**//RHF/3-21G		DFT/B3LYP/6-31G**//RHF/3-21G		
	mech A	mech B	mech A	mech B	mech A	mech B	exptl
reactant	0.0	0.0	0.0	0.0	0.0	0.0	0
TS	43.2 (38.6)	67.1	37.7 (38.2)	48.7	23.6 (21.9)	34.6	15
product	5.2	9.5	−8.3	−8.9	4.9	2.8	1

[a] Experimental values are free energies obtained by the application of transition-state theory to the rates given in ref 4. The calculated values do not include zero-point energy or entropy effects. The values given in parentheses are for the transition state obtained with the tighter optimization criteria. All energies are given in kilocalories per mole.

zinc. Parts c−f of Figure 8 depict the LMOs of the oxygen atom that are significantly different for the reactant and transition state structures. For the reactant structure, (c) represents a lone pair on the oxygen atom and (e) represents a C_D−O σ bond. In contrast, for the transition state structure (d) and (f) represent a nearly fully formed C_D−O double bond (i.e., two nearly equivalent LMOs including both σ and π character). Parts g and h of Figure 8 depict the LMOs representing the O−H bond and are similar for the reactant and transition state structures. Parts i and j of Figure 8 depict the LMOs directly involved in the hydride transfer reaction. As for mechanism A, in the reactant this orbital represents a standard C_D−H bond, while in the transition state this orbital represents a two-electron three-center C_D−H−C_A bond. To summarize, this LMO analysis indicates that in the transition state one of the lone pairs on the oxygen atom combines with the C_D−O σ bond to form a nearly complete C_D−O double bond. This observation provides an explanation for our inability to find an intermediate product state for mechanism B in which the proton relay has not yet occurred. In other words, the completion of the double bond occurring very soon after the transition state induces the deprotonation of the alcohol.

These calculations provide an explanation for the lower overall energy of the reaction path in mechanism A than in mechanism B. In mechanism A the lone pair orbitals on the oxygen atom interact favorably with the zinc throughout the reaction, while in mechanism B the lone pair orbitals on the oxygen atom do not experience such favorable interactions. This difference is confirmed by a CHELPG charge analysis for the transition state structures. For mechansim A the charge on zinc is 0.795 and the charge on the ligating oxygen atom is −0.640. For mechanism B the charge on zinc is 0.586 and the charges on the substrate oxygen and hydrogen are −0.364 and +0.211, respectively. In addition, the Zn−O distance is 1.93 Å in mechanism A and 5.11 Å in mechanism B. Thus, the stabilizing electrostatic interaction between the zinc and substrate is much greater for mechanism A than for mechanism B. This effect is found in the reactant and product structures as well as the transition state structures. These calculations suggest that stabilization by the zinc is at least partly responsible for the lower overall energy of the reaction path of mechanism A relative to that of mechanism B.

These results also provide an explanation for the lower activation energy barrier for hydride transfer in mechanism A than in mechanism B. Figures 7 and 8 indicate greater C_D−O double bond character in the transition state for mechanism B than for mechanism A. This difference suggests that mechanism A exhibits an earlier, more alcohol-like transition state than mechanism B. (Note that the smaller degree of double bond character in the transition state for mechanism A is due in part to the competing interaction of the lone pair oxygen orbitals with zinc in mechanism A.) The earlier transition state is also indicated by the smaller C_D−H distance in the transition state for mechanism A (1.30 Å) than for mechanism B (1.35 Å) and by the smaller angle δ for the secondary hydrogen on the substrate alcohol in the transition state for mechanism A (112.6°) than for mechanism B (115.6°). This angle δ, which is defined in Figure 3, provides an indication of the hybridization of C_D, where smaller values indicate a more alcohol-like transition state. Typically an earlier transition state indicates a lower energy barrier for reaction. Thus, this earlier transition state, which is caused in part by the interaction of the substrate oxygen with the zinc, provides an explanation for the lower barrier in mechanism A than in mechanism B. In addition to energetic considerations, experimental studies indicating an early, alcohol-like transition state for benzyl alcohol oxidation by yeast alcohol dehydrogenase support mechanism A over mechanism B.[48−52]

To examine the dynamical effects of the solvent and enzyme, we performed classical molecular dynamics simulations on the solvated LADH dimer prepared as described above. We performed two different types of classical molecular dynamics simulations. In the first type of simulation (MD1), which is relevant to mechanism A, the hydride is still on the substrate but the proton is no longer on the substrate (i.e., subsequent to the proton relay but prior to the hydride transfer). In the second type of simulation (MD2), which is relevant to mechanism B, both the hydride and the proton are still on the substrate (i.e., prior to both the proton relay and the hydride transfer). As shown in Figure 9, for MD1 the average C_D−C_A distance for the hydride transfer step is 3.56 Å, while for MD2 the average C_D−C_A distance for the hydride transfer step is 4.03 Å. We also observed that for MD1 the average Zn−O distance is 1.84 Å, while for MD2 the average Zn−O distance is 2.01 Å. (Note that these distances are shorter than those observed in the electronic structure calculations described above due to inclusion of the entire solvated enzyme.) The shorter Zn−O distance for MD1 is due to the stronger interaction of the alkoxide than the alcohol with zinc. This stronger Zn−O interaction restricts the motion of the substrate and thus leads to a shorter average C_D−C_A distance. Furthermore, the shorter C_D−C_A distance decreases the barrier for hydride transfer. Thus, these molecular dynamics simulations are consistent with the hypothesis that the deprotonation of the substrate facilitates the hydride transfer step.

We also analyzed the NAD^+ bending motion during the molecular dynamics simulations. We found that for mechanism A $\alpha_C = 1.4° \pm 4.6°$ and $\alpha_N = 2.6° \pm 4.5°$ (where these angles are defined in Figure 3 and the estimated errors are the standard rms deviations). These values are close to those obtained from our electronic structure calculations on the reactant structure for the 148-atom model, as shown in Table 3. Note that our

(48) Klinman, J. P. *J. Biol. Chem.* **1972**, *247*, 7977.
(49) Klinman, J. P. *Biochemistry* **1976**, *15*, 2018.
(50) Welsh, K. M.; Creighton, D. J.; Klinman, J. P. *Biochemistry* **1980**, *19*, 2005.
(51) Cha, Y.; Murray, C. J.; Klinman, J. P. *Science* **1989**, *243*, 1325.
(52) Rucker, J.; Klinman, J. P. *J. Am. Chem. Soc.* **1999**, *121*, 1997.

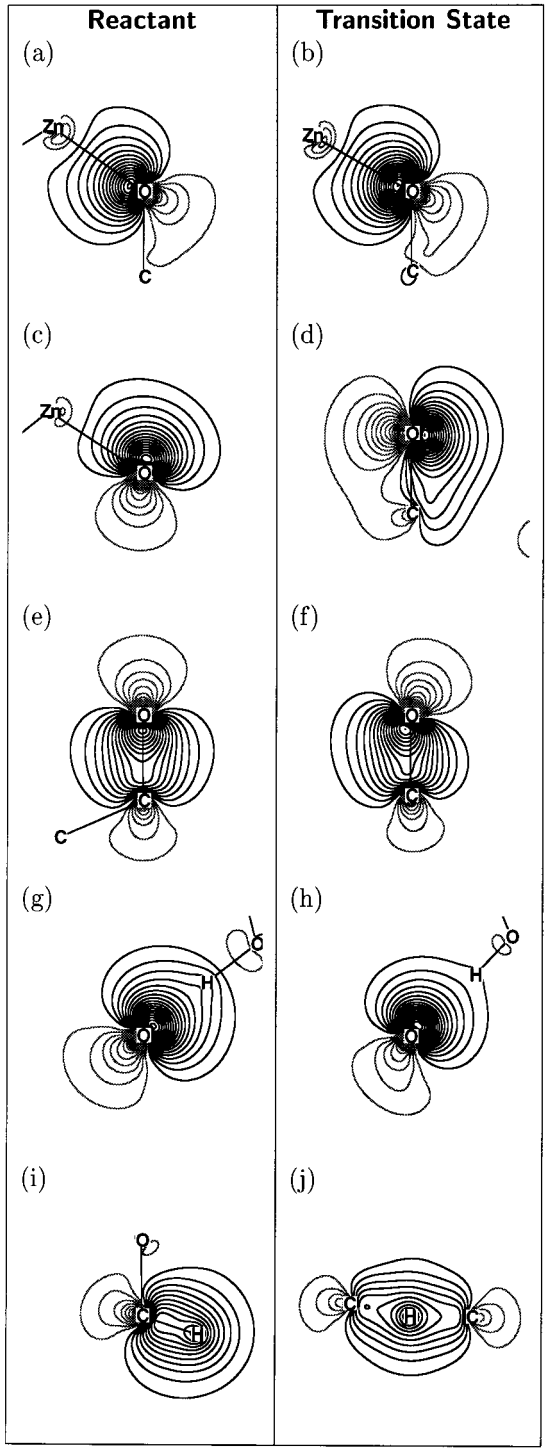

Figure 7. Localized molecular orbitals obtained at the RHF/3-21G level for mechanism A. The left and right columns depict LMOs for the reactant and transition state structures, respectively. The LMOs are identified as follows: (a) and (b) represent lone pairs on the substrate oxygen directed at the zinc; (c) and (d) represent a lone pair on the oxygen and a partial C_D-O π bond, respectively; (e) and (f) represent C_D-O σ bonds; (g) and (h) represent lone pairs on the oxygen hydrogen-bonding to Ser48; (i) and (j) represent a C_D-H bond and a two-electron three-center C_D-H-C_A bond, respectively.

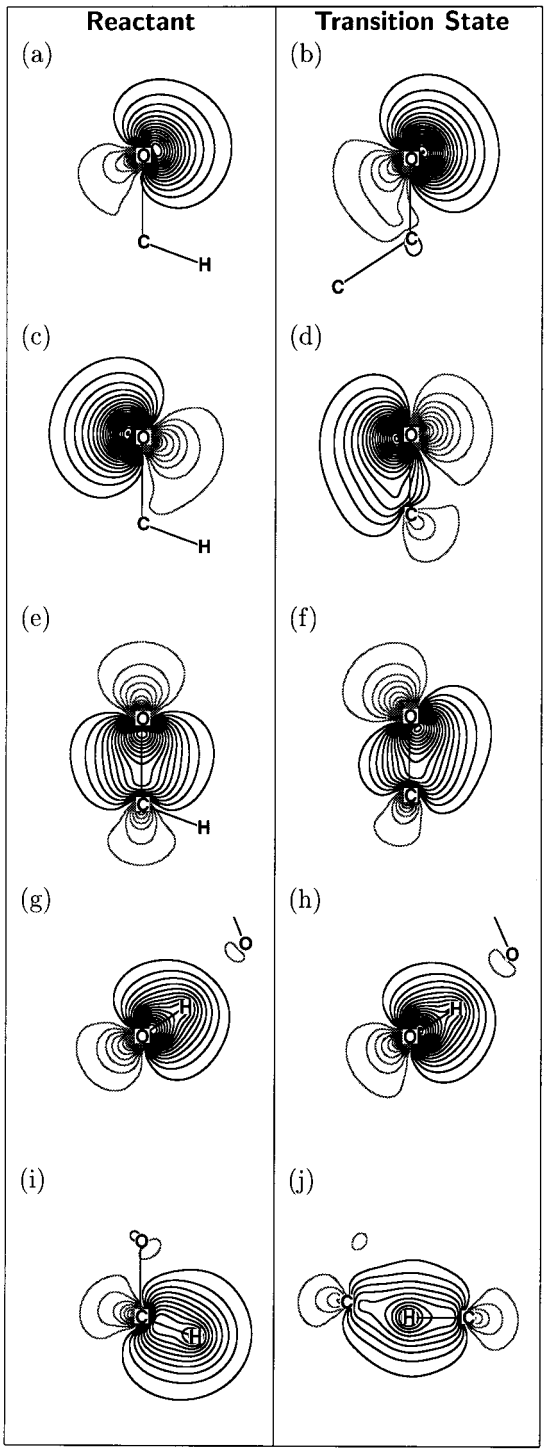

Figure 8. Localized molecular orbitals obtained at the RHF/3-21G level for mechanism B. The left and right columns depict LMOs for the reactant and transition state structures, respectively. The LMOs are identified as follows: (a) and (b) represent lone pairs on the substrate oxygen; (c) and (d) represent a lone pair on the oxygen and half of a double C_D-O bond, respectively; (e) and (f) represent a C_D-O σ bond and half of a double C_D-O bond, respectively; (g) and (h) represent $O-H$ bonds; (i) and (j) represent a C_D-H bond and a two-electron three-center C_D-H-C_A bond, respectively.

molecular dynamics simulations involved only NAD^+, which is expected to be nearly planar, in contrast to the ring puckering of NADH, which has been studied by Wu and Houk[44] and by Almarsson and Bruice.[53]

(53) Almarsson, Ö.; Bruice, T. C. *J. Am. Chem. Soc.* **1993**, *115*, 2125.

Conclusions

In this paper we presented calculations aimed at elucidating the mechanism of the oxidation of benzyl alcohol by LADH. Our calculations support the hypothesis that alcohol deprotonation (i.e., the proton relay) occurs prior to the hydride transfer

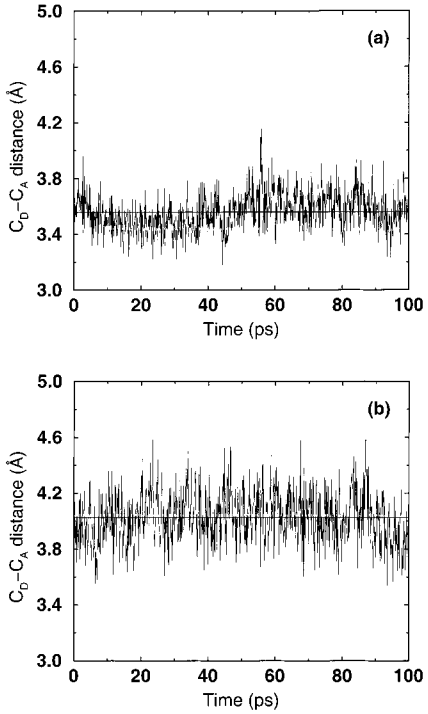

Figure 9. Time evolution of the distance C_D-C_A between the donor and acceptor carbon atoms for the hydride transfer reaction calculated with classical molecular dynamics simulations for (a) mechanism A and (b) mechanism B. The average distance is indicated with a horizontal line.

step and that the alcohol deprotonation facilitates the hydride transfer by lowering the barrier for hydride transfer. Our calculations also indicate that the reactant state is a zinc-bound alkoxide with a strong hydrogen bond to Ser48 and that hydride transfer is accompanied by a weakening of this hydrogen bond. Furthermore, our detailed analysis provides insight into the electronic and dynamical factors governing the charge-transfer reactions in LADH.

The electronic structure calculations on a 148-atom model of the active site indicate that the overall energy of the reaction path and the activation energy barrier for hydride transfer are lower for the mechanism in which the proton relay occurs prior to the hydride transfer step than for the alternative mechanism in which the hydride transfer step occurs first. A thorough analysis of the localized molecular orbitals, the structures, and the partial charges was performed to elucidate these differences. This analysis suggests that the overall energy of the reaction path for hydride transfer after the proton relay is significantly decreased by the stabilizing electrostatic interaction between the alkoxide oxygen and the zinc in the active site. Moreover, the interaction of this oxygen with the zinc competes with the formation of the C_D-O double bond required for the formation of the aldehyde product. This competition results in an earlier, more alcohol-like transition state and thus a lower activation energy barrier for the alkoxide substrate than for the alcohol substrate.

The classical molecular dynamics simulations on the entire solvated LADH dimer indicate that the average distance between the donor and acceptor carbon atoms for the hydride transfer step is significantly smaller after the proton relay than before the proton relay. The shorter donor−acceptor distance after the proton relay is due to the stronger electrostatic interaction of the alkoxide than the alcohol with the zinc, which restricts the motion of the substrate. The activation energy barrier for hydride transfer decreases as the donor−acceptor distance decreases. Thus, the classical molecular dynamics simulations are consistent with the hypothesis that the alcohol deprotonation lowers the barrier for hydride transfer.

In this paper we have neglected nuclear quantum effects, which have been shown to be important for alcohol dehydrogenase reactions.[51,54−58] In another paper we use the active site model introduced in this paper to investigate the nuclear quantum effects for the hydride transfer step of the LADH-catalyzed alcohol oxidation.[59] Future work will focus on mixed quantum/classical molecular dynamics simulations[60] of this reaction in the presence of the entire solvated LADH dimer.

Acknowledgment. We are grateful for financial support from the NIH, Grant GM56207, the NSF CAREER program, Grant CHE-9623813, and the Clare Boothe Luce Foundation. S.H.-S. is the recipient of a Ralph E. Powe ORAU Junior Faculty Enhancement Award, an Alfred P. Sloan Foundation Research Fellowship, and a Camille Dreyfus Teacher−Scholar Award. P.K.A. acknowledges a grant from the Farabaugh Fund for Graduate Research in Substance Abuse from the Univeristy of Notre Dame.

Supporting Information Available: Results of the basis set study for the 43-atom model, structures of the reactant, transition state, and product for the 148-atom model at the RHF/3-21G level for mechanism A, and structures of the reactant and transition state for the 148-atom model at the RHF/3-21G level for mechanism B (PDF). This material is available free of charge via the Internet at http://pubs.acs.org.

JA994456W

(54) Bahnson, B. J.; Park, D.-H.; Kim, K.; Plapp, B. V.; Klinman, J. P. *Biochemistry* **1993**, *32*, 5503.
(55) Bahnson, B. J.; Colby, T. D.; Chin, J. K.; Goldstein, B. M.; Klinman, J. P. *Proc. Natl. Acad. Sci. U.S.A.* **1997**, *94*, 12797.
(56) Bahnson, B. J.; Klinman, J. P. *Methods Enzymol.* **1995**, *249*, 374.
(57) Kohen, A.; Klinman, J. P. *Acc. Chem. Res.* **1998**, *31*, 397.
(58) Kim, Y.; Truhlar, D. G.; Kreevoy, M. M. *J. Am. Chem. Soc.* **1991**, *113*, 7837.
(59) Webb, S. P.; Agarwal, P. K.; Hammes-Schiffer, S. Submitted for publication.
(60) Hammes-Schiffer, S. *J. Phys. Chem. A* **1998**, *102*, 10443.